Astron. Astrophys. 330, 265–276 (1998)

ASTRONOMY
AND
ASTROPHYSICS

Spectral analyses of late-type [WC] central stars of planetary nebulae: more empirical constraints for their evolutionary status⋆

U. Leuenhagen[1,⋆⋆] **and W.-R. Hamann**[2]

[1] Institut für Astronomie und Astrophysik der Universität Kiel, D-24098 Kiel, Germany
[2] Lehrstuhl Astrophysik der Universität Potsdam, Postfach 601553, D-14415 Potsdam, Germany (wrh@astro.physik.uni-potsdam.de)

Received 15 July 1997 / Accepted 22 September 1997

Abstract. The optical spectra of the five recently observed late-type Wolf-Rayet central stars He 2–459 ([WC8]), M 2–43 ([WC8]), SwSt 1 ([WC9]), PM 1–188 and IRAS 21282+5050 (both [WC11]) are analyzed by means of spherically expanding model atmospheres. The stellar parameters T_* (effective temperature), v_∞ (final velocity of the wind), R_* (stellar radius) and $\dot{M}$ (mass loss rate) are determined by NLTE simulations which account for the elements hydrogen, helium, carbon and oxygen. With two exceptions (SwSt 1 and IRAS 21282) the results presented here fit into the sample of already examined [WCL]-type objects. Altogether 13 out of 17 known [WCL]-CSPN have been analyzed so far. The presence of hydrogen in the atmospheres of [WC11] and [WC12] stars becomes more and more evident. In five out of seven analyzed objects of these subtypes hydrogen emission features of stellar origin can be identified.

The spectra of the latest subtypes ([WC11], [WC12]) show rather narrow lines and thus allow to detect features of nitrogen (N II, N III), neon (Ne I) and silicon (Si III, Si IV). For the first time we present model calculations accounting for these elements and perform abundance estimates for the eight narrow-lined stars (all [WC11] and [WC12] plus SwSt 1). The obtained surface compositions are discussed in the light of recent evolutionary calculations which account for diffuse mixing during thermal pulses on the Asymptotic Giant Branch.

Key words: stars: abundances – atmospheres – evolution – mass loss – AGB and post-AGB – Wolf-Rayet

1. Introduction

The spectral class of Wolf-Rayet central stars of planetary nebulae is a small but important group of stellar objects which might be connected as well to the youngest post-AGB stars (proto-planetaries) or to the much older PG 1159 stars at the hottest tip of the post-AGB evolution.

Up to now about 40 galactic objects are classified as [WR] central stars, all of subclass [WC] (Tylenda et al. 1993). Using the classification criteria of Smith (1968), Méndez & Niëmela (1982) and Hu & Bibo (1990) the sample with safe classifications covers mainly the subtypes [WC2]–[WC4] and [WC8]–[WC12], leaving out a gap in which only three objects are found up to now (Acker et al. 1996a; Hamann 1996). Another 11 objects are preliminary classified as "[WC4–6]" for which better spectra are necessary to clarify the situation (cf. Jeffery et al. 1996). The group of stars covering the subtypes [WC8]–[WC12] is called [WC]-late or [WCL]. 17 [WCL] objects are known so far. Leuenhagen & Hamann (1994, hereafter Paper I) and Leuenhagen et al. (1996, hereafter Paper II) have already analyzed eight of these objects (NGC 40, He 2–99, BD+30°3639, CPD−56°8032, He 2–113, M 4–18, K 2–16, V 348 Sgr). In this work we present the results of the spectral analyses of a further five [WCL]-type central stars (He 2–459, M 2–43, SwSt 1, PM 1–188, IRAS 21282+5050).

The characteristics of the spectral classification WC are the strong emission features of helium, carbon and oxygen which are broadened due to the velocities in the stellar wind. Prior studies – and also the work presented here – show that the final velocity of the stellar wind is correlated with the effective temperature. As far as we know from our analyses the effective temperatures of WR-CSPN lie between 20 kK (subtype [WC12]) and 140 kK ([WC2]) and the final velocities cover the range between 200 ([WC12]) and 3000 km s^{-1} ([WC2]). Corresponding to this wide range of parameters the spectral appearance of the various subtypes is, of course, very different. Whereas in the hotter objects features of He II, C IV and the oxygen ions O V to O VII can be detected, the spectra of the latest subtypes are dominated by lines from neutral or singly ionized matter (e.g. He I, C II, O II, Ne I). Due to the enormous broadening in the winds of the early-type objects only the strongest emission lines of the above mentioned ions can be observed. Moreover, closed line blends are completely merged together.

Send offprint requests to: W.-R. Hamann

⋆ Partly based on observations obtained at the German-Spanish Astronomical Center, Calar Alto, Spain

⋆⋆ *Present address:* I. Physikalisches Institut, Universität Köln, Zülpicher Str. 77, D-50937 Köln, Germany (leuen@ph1.uni-koeln.de)

The lower the wind velocities the narrower the lines. This way, in the latest subtypes ([WC11], [WC12]) weak features of trace elements also become visible. If high quality spectra (1 Å resolution at optical wavelengths or better) are available, these emission or absorption lines can be used for a study of the involved element. In this paper we present trace element analyses of the elements nitrogen, neon and silicon for the peculiar [WC9] object SwSt 1 (peculiar because of the slow wind velocity) and the seven [WC11] and [WC12] stars PM 1–188, CPD−56°8032, He 2–113, M 4–18, K 2–16, IRAS 21282+5050 and V 348 Sgr.

Within this paper Sect. 2 provides general information about the observational data and the recently analyzed stars. The model calculations and atomic data are described in Sect. 3. Sect. 4 contains the spectral fits and resulting parameters for the recently analyzed objects and detailed information about the hydrogen and trace element analyses. In Sect. 5 some comments on the results can be found. The evolutionary status of [WCL]-type stars is discussed in Sect. 6 and a summary can be read in Sect. 7.

2. The recently analyzed stars

2.1. Observations

In order to resolve also the weaker and narrower lines of the latest subtypes it is necessary to apply spectrograms with a spectral resolution of 1 Å or better. The optical spectra of the five newly analyzed objects were collected at the DSAZ, Calar Alto, Spain, using the 3.6m telescope and the TWIN spectrograph (Tek-CCD, 1.″8 slit). The covered wavelength regions are 3800–5000 Å and 5500–6700 Å (for M 2–43 only 4350–5000 Å and 6100–6700 Å). The data reduction was carried out with the IRAF software. The raw spectra were divided by a continuum fit of standard stars (BD−9 4395, BD+25 3941, BD+28 4211) in order to level out the frequency dependence of the instrumental response. Finally each spectrum was rectified by fitting a low-order polynomial through hand-selected points of the suspected continuum. Nebula contributions, as well lines as continuum, are not subtracted at all. We use the observed wavelengths of the nebular emission lines for determining a correction for the radial velocity of each object.

Several kinds of features are visible in the observed spectra.

- Emission features formed in the stellar wind. These features are the basis for our spectral analyses. The lines of H, He, C and O are broadened due to the motion in the expanding stellar atmosphere. Some of the emissions are accompanied by blue-shifted absorption features (so-called P-Cygni profiles).
- Narrow emissions (Hα, Hβ, [N II] and partly He I, C II and [Fe III]) which are formed in the planetary nebula. The line shape reflects mainly the instrumental profile which we suppose to have Gaussian shape.
- A third kind of spectral features is due to interstellar absorption. Most prominently, the Na I D multiplet (rest wavelengths at 5890 and 5896 Å) is clearly visible in all spectra, shifted individually by the velocities of interstellar clouds. In the spectra of He 2–459 four different components can be identified (Fig. 1).

2.2. The program stars

He 2–459 (PN G 068.3−02.7)

He 2–459 was catalogued by Henize in 1967 and is classified as [WC8]. From radio maps Aaquist & Kwok (1990) determined the diameter of the planetary nebula to 1.″3. UBV magnitudes of $m_{\rm U} = 15\overset{\rm m}{.}12$, $m_{\rm B} = 14\overset{\rm m}{.}10$ and $m_{\rm V} = 12\overset{\rm m}{.}67$ were given by Nicolet (1978). Cahn et al. (1992) found a Shklovsky distance of 3.4 kpc, and an extinction constant of $C = 2.7$ ($E_{\rm B-V} = 0\overset{\rm m}{.}85$) is measured by Tylenda et al. (1992) from the Balmer decrement.

M 2–43 (PN G 027.6+04.2)

The subtype of M 2–43 (alias MA 9) is again [WC8]. Indeed, the spectral appearance is very similar to He 2–459 but the brightness of this central star is considerably smaller ($m_{\rm V} = 15\overset{\rm m}{.}7$, Acker et al. 1992). Aaquist & Kwok (1990) measured a nebula diameter of 1.″5 and Cahn et al. (1992) determined a distance of 1.4 kpc (Shklovsky method). A relatively high extinction constant of $C = 4.0$ ($E_{\rm B-V} = 1\overset{\rm m}{.}26$) is published by Tylenda et al. (1992). From an analysis of the nebula Preite-Martinez et al. (1989) derived a central star temperature of $T_{\rm EB} = 73.4$ kK (energy balance method).

SwSt 1 (PN G 001.5−06.7)

This somewhat peculiar object was already discovered by Swings & Struve (1943). SwSt 1 (alias HD 167362, [WR23] or He 2–377) is the brightest star in the analyzed sample ($m_{\rm V} = 11\overset{\rm m}{.}9$, $m_{\rm B} = 12\overset{\rm m}{.}1$). In the literature this object is classified as [WC10] or Of-WR(C). Taking the C II:C III:C IV line strength ratio of our spectra SwSt 1 must be classified as [WC9], however, the line strengths are unusually small compared to other [WC9] objects like BD+30°3639 or He 2–99 (cf. Paper II).

The planetary nebula of SwSt 1 has a diameter of 1.″3 (Aaquist & Kwok 1990) and the Shklovsky distance is 1.4 kpc (Cahn et al. 1992). Concerning the reddening towards this object one can find controversial results. Tylenda et al. (1992) use the Balmer decrement for determining an extinction constant of $C = 0.7$ ($E_{\rm B-V} = 0\overset{\rm m}{.}22$), Zijlstra et al. (1991) mentioned a reddening of $E_{\rm B-V} = 0\overset{\rm m}{.}75$, Zhang & Kwok (1991) found $E_{\rm B-V} = 0\overset{\rm m}{.}35$, de Freitas Pacheco & Veliz (1987), who presented an analysis of the physical conditions in SwSt 1, gave $E_{\rm B-V} = 0\overset{\rm m}{.}41$ and Flower et al. (1984) derived $c = 0.35$ ($E_{\rm B-V} = 0\overset{\rm m}{.}25$) from flattening the 2200 Å feature and $c = 0.50$ ($E_{\rm B-V} = 0.36$) using radio data and the Hβ line strength. By comparing absolute calibrated IUE spectra with our model flux for SwSt 1 we derived a reddening close to the value of de Freitas Pacheco & Veliz.

Several authors use the strengths of the nebula lines for determining a temperature for the central star. Zhang & Kwok

(1991) found a Zanstra temperature of T_Z (H I) = 32 kK, Grewing & Neri (1990) derived T_{UV} = 34 kK from UV color indices and a Zanstra temperature of T_Z (H I) = 35.5 kK, Preite-Martinez et al. (1989) found T_{EB} = 26.6 kK and Flower et al. (1984) derived T_Z = 36 kK and T_S = 30–36 kK (Stoy method) from their nebula analysis.

A comparison of the line widths of several WC9 stars including SwSt 1 is presented by Méndez et al. (1991). Their sample consists of both WR-CSPN and Pop. I objects but no spectral differences belonging to the different masses could be found. Cerruti-Sola & Perinotto (1985) derived a final velocity of the stellar wind of 1950 km s^{-1} and gave an estimation for the mass loss rate (5 10^{-8} $M_\odot$ yr^{-1}) from analyzing low-resolution IUE spectra of SwSt 1.

PM 1–188 (PN G 012.2+04.9)

PM 1–188 was first discovered by the IRAS satellite and described as "probable PN" by Preite-Martinez (1988). Later, Hu & Bibo (1990) classified this object (also called HuBi 1 or IRAS 17514−1555) correctly as [WC11] central star. Hu & Bibo published a list of identified emission features in the optical spectrum and photometric data exposing a strong infrared excess. From a CCD image of the object they derived a nebula diameter of 10″. In contradiction to this value Pollacco & Hill (1994) found a diameter of 18″. From the nebula spectrum the latter authors determined a reddening of E_{B-V} = 0.^{m}83 using the Balmer line method. If both the stellar and nebula spectrum are considered the reddening is reduced to 0.^{m}25. The lower value is consistent with the result of Zijlstra et al. (1991) who mentioned E_{B-V} = 0.^{m}15.

IRAS 21282+5050 (PN G 094.0−00.1)

Since its discovery by the IRAS satellite a remarkably large number of publications has been based on this object. Most of the research is focused on the circumstellar shell whose spectrum shows strong PAH features and lines of molecules such as H_2, CO, ^{13}CO or HCO$^+$ (cf. Shupe et al. 1994; Likkel & Meixner 1994; Likkel et al. 1988). Observations in the wavelength range 2.4–17 μm by the ISO satellite were presented and discussed by Beintema et al. (1996) and Molster et al. (1996). The reddening towards IRAS 21282 is very strong (E_{B-V} = 1.^{m}9, Cohen & Jones 1987) and mostly due to the circumstellar material. Cohen & Jones (1987) and Kwok et al. (1993) published photometric data and the latter authors compared this object with other [WCL]-type central stars and assessed the dynamical age of the PN to 10^3 years. Optical images show an extension with size of 6.″5 × 4.″8 (elongation along the N-S direction). From the radial velocity of IRAS 21282 Likkel et al. (1988) estimated the distance to 2 kpc at maximum.

3. The model calculations

The model calculations are based on the assumptions of homogeneity and stationarity. The atmospheres are supposed to be spherical. The depth dependence of the (supersonic) wind velocity is parametrized by $v(r) = v_\infty\,(R_* - 1/r)$. The final velocity v_∞ is a free parameter which can be fixed by measuring the most blue-shifted absorption component of the observed P-Cygni profiles. Both the velocity field and mass-loss rate define the density stratification via the equation of continuity. Further free parameters are the effective temperature T_*, the stellar radius R_* (luminosity: $L = 4\pi R_*^2\,\sigma T_*^4$) and the chemical composition.

Table 1. Number of NLTE levels considered within the different ionization stages of the trace elements nitrogen, neon and silicon.

nitrogen				neon		silicon		
I	II	III	IV	I	II	III	IV	V
3	28	26	6	8	1	24	7	1

Stellar radius, mass-loss rate and final velocity define the *transformed radius* R_t by $R_t = R_*(v_\infty/\dot{M})^{2/3}$ with v_∞ in units of 2500 km s^{-1} and $\dot{M}$ in units of 10^{-4} $M_\odot$ yr^{-1}. The analysis procedure is simplified by the empirical fact that two models with equal R_t but different $\dot{M}$ and R_* exhibit nearly identical emergent spectra (Schmutz et al. 1989; Hamann et al. 1992). R_t can be used as tracer for the reciprocal wind density.

The radiation transfer equation is solved by the "co-moving frame (CMF)" technique of Mihalas et al. (1975). The simultaneous solution of the equations of statistical equilibrium (non-LTE case), augmented by the radiative equilibrium constraint, and the radiation transfer problem is performed by the Accelerated Lambda Iteration (ALI) technique.

The five stars mentioned in Sect. 2.2 are analyzed using model atmospheres consisting of the elements hydrogen, helium, carbon and oxygen. The model atom of each element depends on the subtypes of the analyzed objects and contains up to 231 non-LTE levels plus 52 LTE levels. A detailed description of the atomic data and more information about the model calculations are given in Paper II.

For the analyses of the trace elements additional model atoms have to be considered. Table 1 shows the numbers of non-LTE levels for each of the ions or atoms used. In the case of singly ionized nitrogen (N II) we further account for 22 LTE levels (autoionizing levels) and 144 stabilizing transitions from these LTE levels as a channel for dielectronic recombination processes. The model atom of neon is quite simple. For each main quantum number singlet and triplet terms are combined. During the calculation of the emergent flux these combined levels are split into sublevels according to the jj-coupling (assuming LTE). The level energies of nitrogen, neon and silicon are taken from Bashkin & Stoner (1975) and the transition probabilities are from the Opacity Project.

4. Results

4.1. Determination of stellar parameters

In this section the results of the spectral analysis of the five [WCL] objects introduced in Sect. 2.2 are presented. The de-

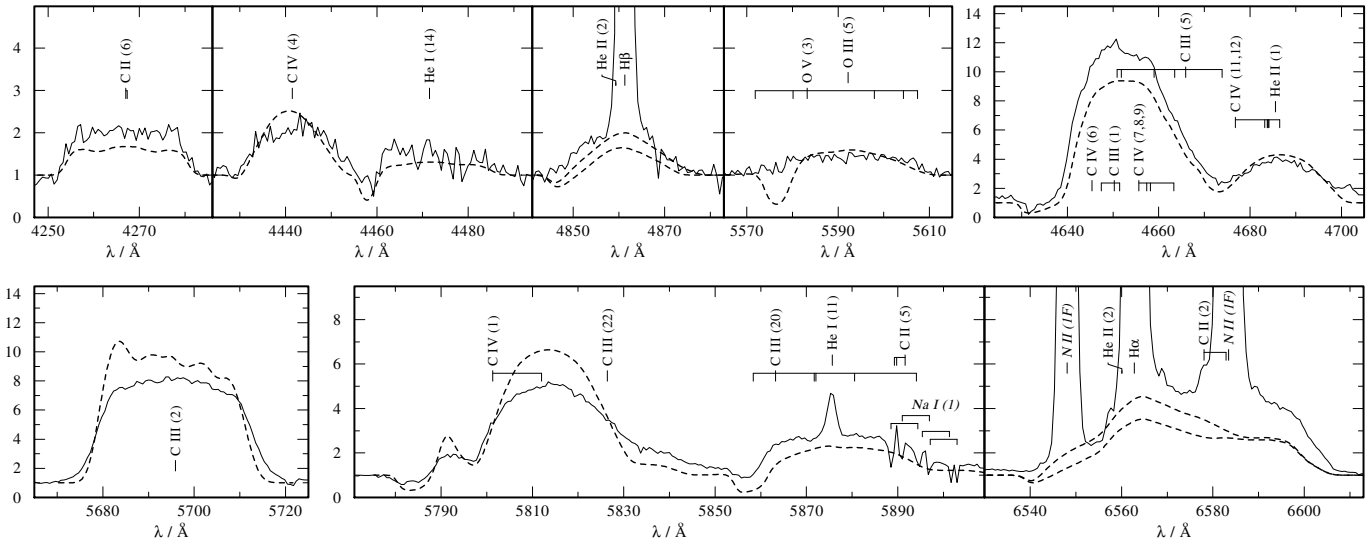

Fig. 1. Observations (solid line) and synthetic spectra (dashed line) of **He 2–459** (subtype [WC8]). Two different models are shown at Hβ and Hα, $\beta_{\rm H} = 0\,\%$ and $4\,\%$ (mass fraction).

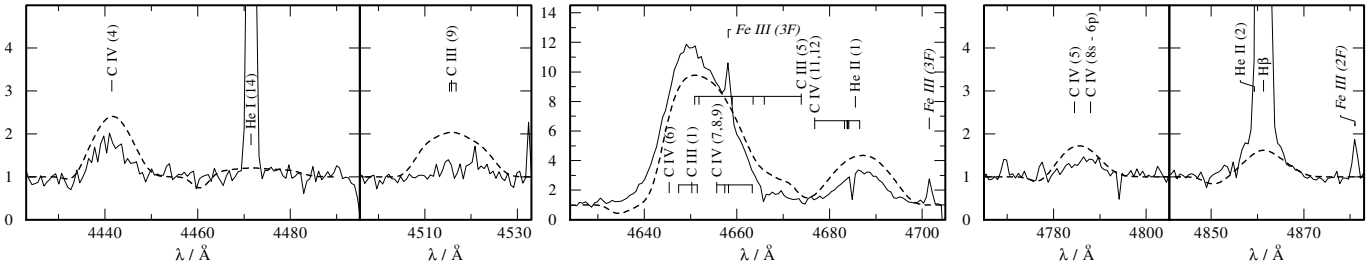

Fig. 2. Observations (solid line) and synthetic spectra (dashed line) of **M 2–43** (subtype [WC8]).

termination of the stellar parameters is based on several optical emission features of hydrogen (if present), helium, carbon and oxygen. The observed spectral ranges contain the most important lines, like Hα, Hβ, several He I and He II lines, the classification lines of carbon, a few O II transitions and the O III/O V blend at 5590 Å. For M 2–43 only a short spectrogram is available to us, which is insufficient to determine the chemical composition. Because of its similarity to the spectrum of He 2–459 we adopt the element abundances from the latter in that case.

In Figs. 1 to 5 the final spectral fits are plotted. The individual model parameters are given in Table 2. All synthetic profiles are convolved with a Gaussian of 1 Å (FWHM). The multiplet numbers in brackets refer to Moore (1959, 1970). Slanted designations identify observed lines which are not included in the model calculations.

The fitting procedure of the observed line profiles provides the effective temperature T_*, the final wind velocity v_∞, the element abundances and the transformed radius $R_{\rm t}$ (cf. Sect. 3). Knowledge of the absolute (visual) brightness is required in order to disentangle $R_{\rm t}$ into the stellar radius R_* and the mass-loss rate $\dot{M}$. By applying the distances d and the color excesses $E_{\rm B-V}$ as quoted in Sect. 2.2 the individual absolute magnitudes of the stars are determined from the apparent magnitudes in the visual (and at other wavelengths, if available). In Table 2 the vertical bar separates the directly determined stellar parameters from those which depend on the adopted distance ($R_* \propto d$, $\dot{M} \propto d^{3/2}$, $L \propto d^2$).

4.2. Determination of the hydrogen abundance

In a previous study (Paper I) a small amount of hydrogen has been detected in the [WC12] star V 348 Sgr. The presence of hydrogen in helium-burnt, carbon-rich material was not expected and poses significant constraints for the evolutionary formation of such objects. Therefore it is extremely interesting to search for traces of hydrogen in other [WCL] stars.

In Wolf-Rayet stars with strong He II lines, the analysis of hydrogen lines is hampered by the fact that every hydrogen line is located close to a He II line, with a separation corresponding to a Doppler shift of 123 km s^{-1} only. If the wind velocities are larger than this separation, the hydrogen lines are not separated from their He II counterparts. Hamann et al. (1991) therefore determined the hydrogen abundance in Population I WN stars from the *excess* emission in helium/hydrogen blends, compared to unblended helium lines of the same series. This method is clearly not sensitive to small traces of hydrogen. In the case

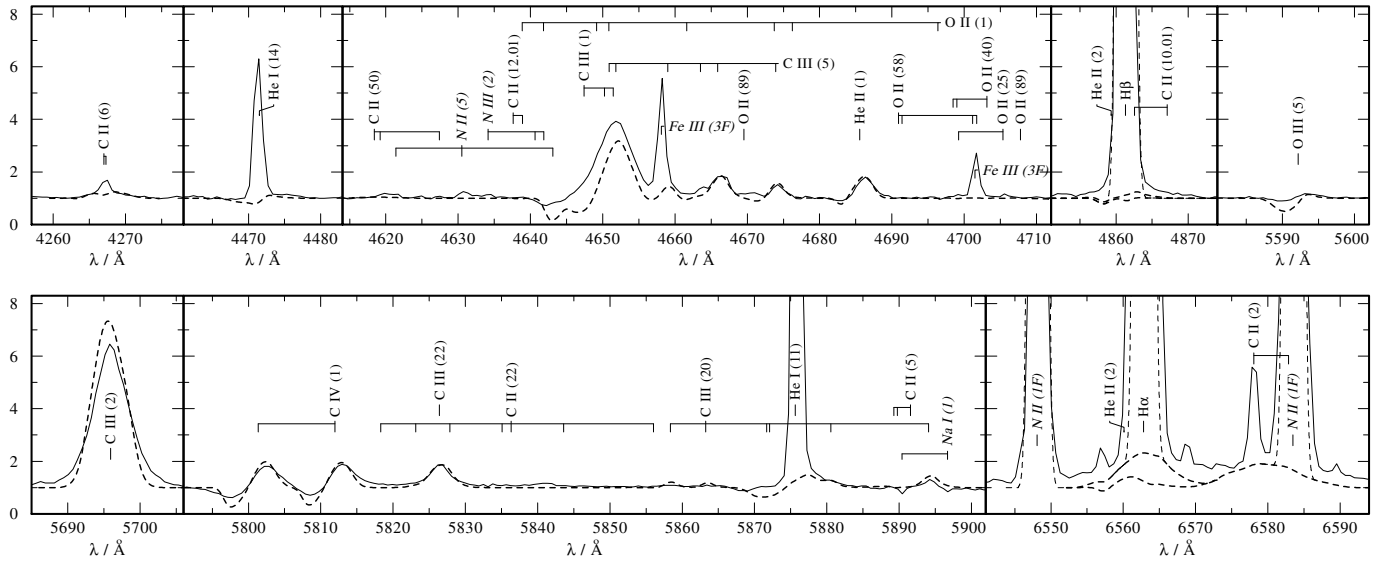

Fig. 3. Observations (solid line) and synthetic spectra (dashed line) of **SwSt 1** (subtype [WC9]). Two different models are shown at Hβ and Hα, $\beta_{\rm H} = 1$ % and 10 % (mass fraction). The thin dashed lines represent Gaussian fits to the nebula lines (Hβ, N II 6548 Å, Hα, N II 6584 Å) which are added to the stellar spectrum. Some nebular lines are saturated. Aside Hα and N II 6584 Å Rowland ghosts at $\Delta\lambda = \pm 5.9$ Å are visible.

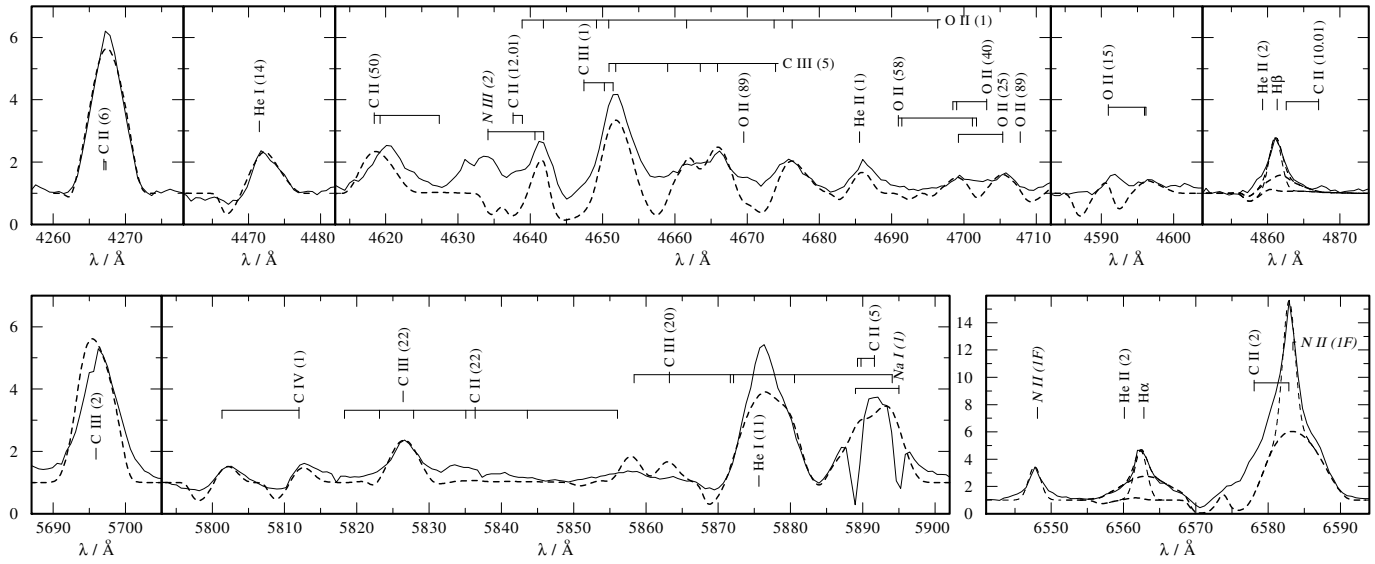

Fig. 4. Observations (solid line) and synthetic spectra (dashed line) of **PM 1–188** (subtype [WC11]). Two different models are shown at Hβ and Hα, $\beta_{\rm H} = 0$ % and 1 % (mass fraction). Thin dashed lines as in Fig. 3.

of central stars the nebular lines (see above) pose an additional difficulty.

Problems of that kind are encountered with early-type [WC] spectra, as well as with [WC8] and [WC9] stars (cf. Fig. 1 and Paper II). In the neighborhood of Hα there are also two strong nitrogen lines and an important C II transition. For these subtypes we only could determine upper limits for the hydrogen abundance.

The situation becomes more favorable for the subtypes [WC11] and [WC12]. First, He II lines are weak or absent in these considerably cooler stars. Moreover, the terminal wind velocity, which is strongly correlated with the subtype, is smaller. Consequently, the features are narrower and the wavelength shift between H I and He II becomes visible. On the other hand, the same effect makes it more difficult to distinguish the nebular hydrogen emission lines from a possible stellar contribution. E.g., in our spectrum of IRAS 21282 (cf. Fig. 5) the stellar emission at 6560 Å is almost completely hidden behind the nebular Hα emission, except of the outer line wings. Observations with a higher spectral resolution would allow us to discriminate the nebular lines better, but are not to our disposal for these rather

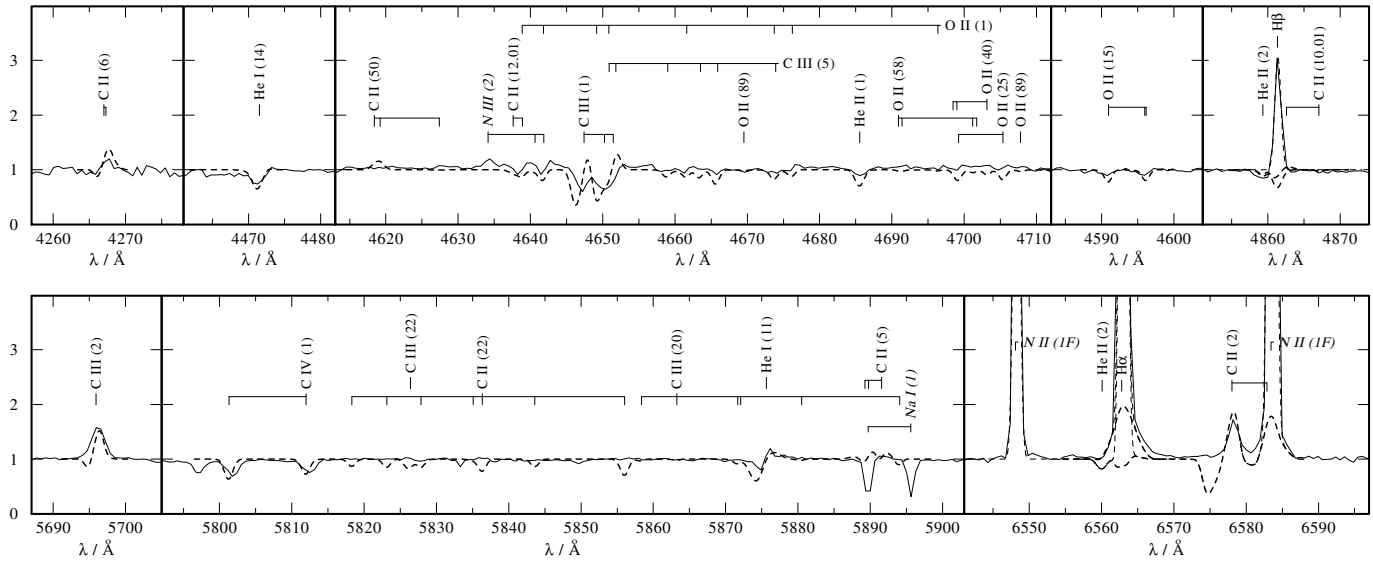

Fig. 5. Observations (solid line) and synthetic spectra (dashed line) of **IRAS 21282+5050** (subtype [WC11]). Two different models are shown at Hβ and Hα, $\beta_{\rm H} = 1.5\,\%$ and $10\,\%$ (mass fraction). Thin dashed lines as in Fig. 3.

Table 2. Parameters of [WCL]-type central stars. $T_{2/3}$ refers to the radius $R\,(\tau_{\rm Ross} = 2/3)$. The definition of the transformed radius $R_{\rm t}$ is given in Sect. 3. Note that all parameters within the vertical bars depend on the adopted distances, brightnesses and reddenings (see Sect. 2.2). The luminosity of PM 1–188 is presumed (distance in brackets follows from $\log L/L_\odot = 3.70$). The element abundances are given in mass fractions ($\beta_{\rm H}$: upper limits in parentheses; M 2–43: taken from He 2–459, see Sect. 4.1).

		stellar parameters				distance dependent results				chemical comp.			
	subtype	T_* [kK]	$T_{2/3}$ [kK]	v_∞ [km s^{-1}]	$R_{\rm t}$ [$R_\odot$]	d [kpc]	R_* [$R_\odot$]	$\log \dot{M}$ [$M_\odot$/yr]	$\log L$ [$L_\odot$]	$\beta_{\rm H}$ [%]	$\beta_{\rm He}$ [%]	$\beta_{\rm C}$ [%]	$\beta_{\rm O}$ [%]
He 2–459	[WC8]	77	54	1000	2.15	3.4	0.84	−5.01	4.37	($\leq$ 2)	40	50	10
M 2–43	[WC8]	65	56	850	4.04	1.4	0.32	−6.08	3.24	($\leq$ 2)	40	50	10
SwSt 1	[WC9]	35	34	400	25.91	1.4	1.03	−6.90	3.27	($\leq$10)	44	53	3
PM 1–188	[WC11]	35	32	360	7.07	(1.5)	1.88	−5.70	3.70	1	42	50	7
IRAS 21282	[WC11]	28	27	180	51.95	<2.0	<3.12	<−6.98	<3.75	10	43	46	1

faint objects. Nebular contamination could also be suppressed with the higher spatial resolution of the HST.

Our technique of handling the nebular blends can be seen in Figs. 4 and 5 (and also in Fig. 12 of Paper II). In the subplots for Hβ and Hα two models with different hydrogen contents in the stellar wind are shown (strong dashed lines). Gaussian profiles (thin dashed lines) are added to the modeled stellar component in order to reproduce the peak heights of the observed nebular emission. In the case of the model with lower hydrogen abundance the *wings* of the observed profile are not fitted. With an appropriate hydrogen content the observed line profile can be reproduced almost perfectly. For checking this method also the unblended [N II] nebular line at 6548 Å is overplotted with a Gaussian of the same FWHM as for the hydrogen lines but this time matching the individual [N II] peak height. Obviously, the wings of the observed [N II] line are fitted without needing an additional stellar component.

Thus we have positively determined traces of hydrogen in both [WC11] stars of our actual sample (cf. Table 2). Up to now hydrogen was definitely detected only in V 348 Sgr ($\beta_{\rm H}$=4 %, Paper I). The supposed presence of hydrogen in the atmospheres of He 2–113 and K 2–16 (Paper II) is now quantitatively confirmed by our current, more refined study (He 2–113: 7 %, K 2–16: 1 % hydrogen). Consequently, from seven [WC11] or [WC12] objects analyzed by us so far only one star (CPD−56°8032) shows definitely *no* indications for any hydrogen (Paper II). In the case of M 4–18 only a rough upper limit can be given because of strong nebular lines and a low-resolution spectra (see also Paper II).

4.3. Analysis of the trace elements N, Ne and Si

The search of trace elements in the atmospheres of [WCL] type objects needs high-resolution, high signal-to-noise spectra. Only some of the spectra available to us are fulfilling these requirements. Furthermore, the detection of weak features is hindered by the broadening due to the motion of matter. Only the latest subtypes, i.e. the objects with slow wind velocities, are good candidates for a trace element analysis. In this work we studied the features of nitrogen, neon and silicon in the spectra of SwSt 1 ([WC9]) and all available [WC11]- and [WC12]-

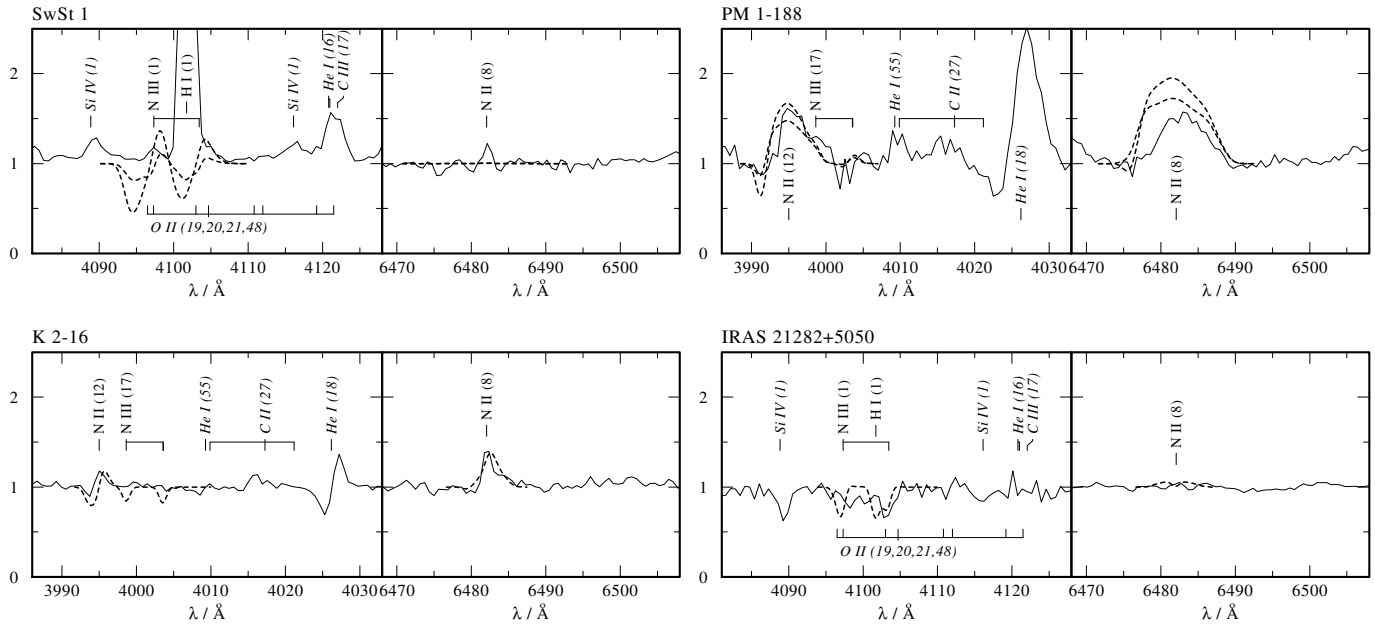

Fig. 6. Observed (solid line) and modeled (dashed lines) **nitrogen** features of **SwSt 1** (upper left, $\beta_N = 0.1\,\%$, $0.5\,\%$), **PM 1–188** (upper right, $\beta_N = 0.5\,\%$, $1\,\%$), **K 2–16** (lower left, $\beta_N = 2\,\%$) and **IRAS 21282** (lower right, $\beta_N = 0.5\,\%$). Slanted designations identify lines which are not included in the model calculations.

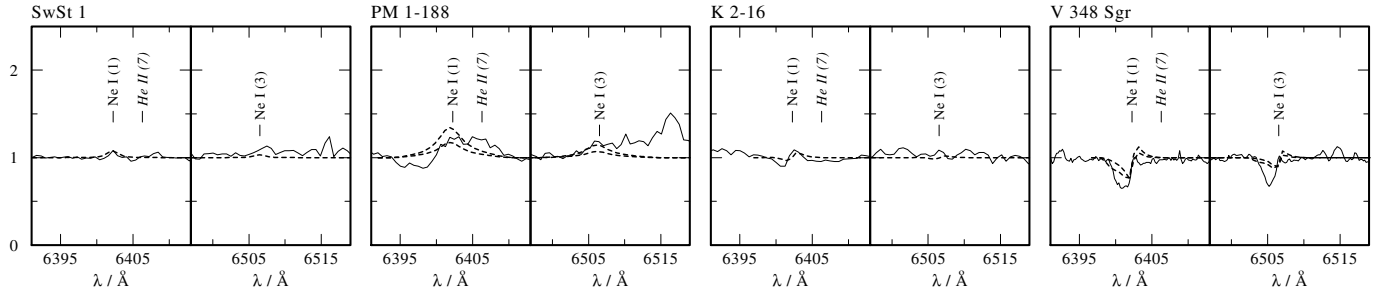

Fig. 7. Observed (solid line) and modeled (dashed lines) **neon** features. From left to right: **SwSt 1** ($\beta_{Ne} = 4\,\%$), **PM 1–188** ($\beta_{Ne} = 2\,\%$, $4\,\%$), **K 2–16** ($\beta_{Ne} = 4\,\%$) and **V 348 Sgr** ($\beta_{Ne} = 1\,\%$, $2\,\%$). Slanted designations identify lines which are not included in the model calculations.

type spectra (PM 1–188, CPD−56°8032, M 4–18, He 2–113, K 2–16, IRAS 21282, V 348 Sgr).

If available we use the unblended multiplets N II (12) 3995 Å, N II (8) 6482 Å and N III (17) 3999, 4004 Å for the nitrogen analysis. Otherwise, an upper limit for the nitrogen content is determined from N III (1) 4097, 4104 Å (blended by Hδ and O II) or N II (5) 4600–4643 Å. Ne I 6402 Å and 6505 Å are used for the neon analysis and Si III (2) 4552, 4568, 4575 Å, Si III (4) 5740 Å and Si IV (1) 4089, 4116 Å serve as tracers for the silicon analysis. In Figs. 6 to 8 a selection of line fits is presented.

In the atmosphere of SwSt 1 ([WC9]) the degree of ionization is considerably higher than in those of the other [WC11] or [WC12] stars. Consequently, the stellar features of N II or Si III are absent, only lines of N III and Si IV are visible. The weak emission at N II (8) 6482 Å (see Fig. 6, upper left) might be of nebular origin. The spectra of PM 1–188 and K 2–16 show quite prominent emissions of singly ionized nitrogen (e.g. N II (8) at 6482 Å) which can be reproduced by model atmospheres containing 1 % nitrogen (mass fraction). In the case of IRAS 21282 and V 348 Sgr only *absorption* features of nitrogen are present.

Comparing our high quality spectra of He 2–113 and CPD−56°8032 significant differences concerning nitrogen can be found. Despite the general similarity of these spectra, only in He 2–113 nitrogen lines are present. The definite absence of nitrogen features in CPD−56°8032 leads to a very small upper limit of $\beta_N < 0.1\%$. It is interesting to note that CPD−56°8032 is the only one of the seven [WC11] or [WC12] objects which shows no indications of hydrogen. This correlation between the lack of hydrogen *and* nitrogen suggests a related origin of these elements.

The *neon* features observed can be scarcely reproduced by the model atmospheres. A neon fraction of at least 2 to 4 % is necessary to match the line strengths. The strongest feature (6403 Å) clearly shows a blue-shifted absorption component indicating a formation depth far out in the wind. Unfortunately,

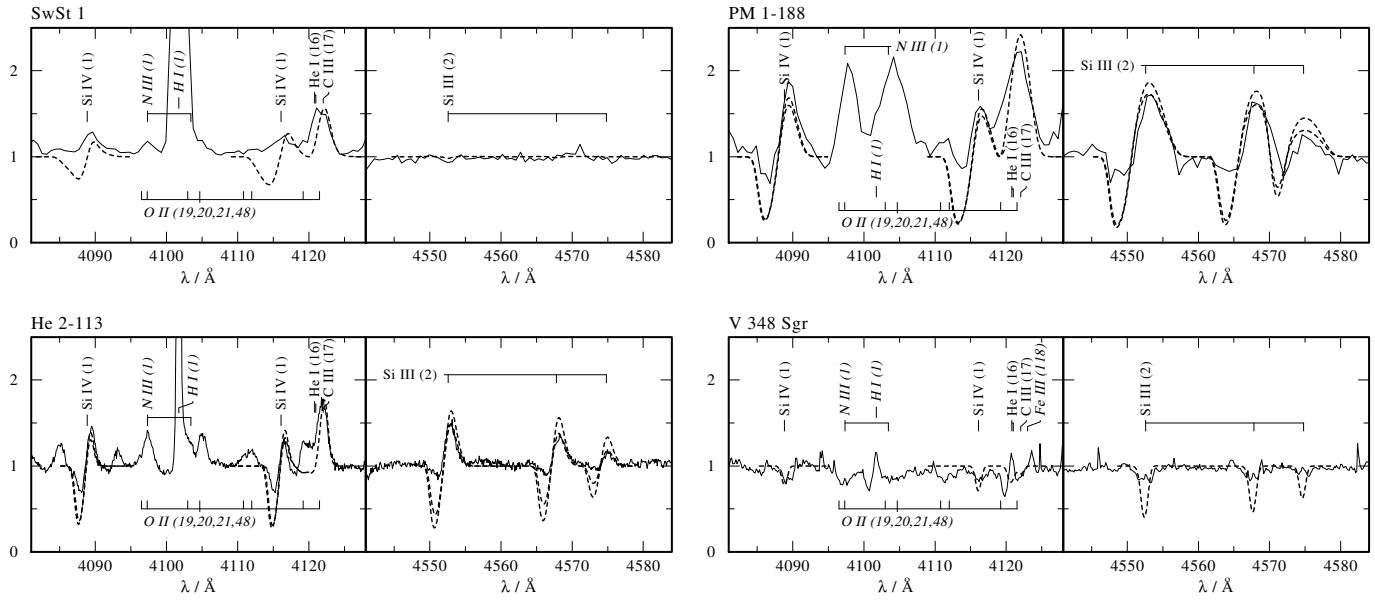

Fig. 8. Observed (solid line) and modeled (dashed lines) **silicon** features of **SwSt 1** (upper left, $\beta_{\rm Si} = 1\,\%$), **PM 1–188** (upper right, $\beta_{\rm Si} = 2\,\%$, $3\,\%$), **He 2–113** (lower left, $\beta_{\rm Si} = 0.5\,\%$, $1\,\%$) and **V 348 Sgr** (lower right, $\beta_{\rm Si} = 0.1\,\%$). Slanted designations identify lines which are not included in the model calculations.

Table 3. Element abundances (mass fractions) of nitrogen, neon and silicon in the atmospheres of [WC] central stars of latest subtypes.

	subtype	T_* [kK]	$\beta_{\rm N}$ [%]	$\beta_{\rm Ne}$ [%]	$\beta_{\rm Si}$ [%]
SwSt 1	[WC9]	37	<0.5	2...4	≈ 1
PM 1-188	[WC11]	35	1	2...4	2...3
CPD$-56°8032$	[WC11]	32	<0.1	$-$[a]	0.5...1
M 4-18	[WC11]	31	<0.5	$-$[a]	0.5...1
He 2-113	[WC11]	30	0.5	$-$[a]	0.5...1
K 2-16	[WC11]	30	1	>4	0.5...1
IRAS 21282	[WC11]	28	<0.5	$-$[b]	<0.1
V 348 Sgr	[WC12]	20	0.5...1	2	<0.1

[a]: no spectra available; [b]: no neon lines detectable

in the case of CPD$-56°8032$, M 4–18 and He 2–113 no observations of neon lines are available to us. Other high resolution spectra of CPD$-56°8032$ and He 2–113 were published by de Marco et al. (1996, 1997) in which a P-Cygni shaped Ne I 6402 Å feature is clearly present. From a comparison with our PM 1–188 spectrum we concluded that the neon abundance in CPD$-56°8032$ and He 2–113 must be similar to that in PM 1–188.

The *silicon* lines are mostly P-Cygni shaped. Except PM 1–188 (2 to 3 %) the observed line strengths are fitted by model atmospheres accounting for 0.5 to 1 % silicon. The low wind density of IRAS 21282 and V 348 Sgr leads to silicon absorption lines whose strengths are already surpassed by the modeled profiles of an atmosphere containing only 0.1 % silicon. All resulting values or upper limits for the element abundances of nitrogen, neon and silicon are compiled in Table 3.

As already mentioned by Leuenhagen et al. (1994) several types of line profiles appear in the spectrum of V 348 Sgr. Pure emissions, pure absorptions, P-Cygni shaped features and some peculiar profiles with a narrow inversion at the rest wavelength can be observed. Some of the transitions, e.g. N II (5) and all Ne I features, appear as blue-shifted absorption lines with a narrow emission component at the rest wavelength (see Fig. 7, most right panel). Jeffery (1995) made an attempt to analyze the absorption spectrum of V 348 Sgr with static LTE model atmospheres. Concerning the peculiar line shapes and the large line widths of the nitrogen features he argued that the profiles are "double-peaked" and that only one "component" should be used for the analysis. Our model calculations include broadening effects due to the velocities in the stellar wind. The synthetic line profiles for V 348 Sgr ($v_\infty = 190\,{\rm km\,s^{-1}}$, Paper I) can still not reproduce the peculiarities but the total line widths can be fitted well.

5. Discussion

Most of the observed spectral features of the newly analyzed stars (emissions as well as absorptions) can be reproduced by the model calculations. In some cases the fit of P-Cygni shaped features of He I, C II, O II or O III fails because the blue-shifted absorption part is overestimated by the models. In the spectrum of SwSt 1 (see Fig. 3) the narrow C II emission peaks at 4267 Å and 6578 Å are of nebular origin.

Especially in the case of the [WC8] objects the determination of the effective temperature and the transformed radius is somewhat tricky, since the grade of ionization in the wind depends not only on T_* but also on the wind density. Focusing only on the line strengths, a small change in T_* can be compen-

Table 4. Zanstra temperatures of the model fluxes.

	subtype	T_* [kK]	T_Z(H I) [kK]	T_Z(He I) [kK]	T_Z(He II) [kK]
He 2–459	[WC8]	77	47	45	16
M 2–43	[WC8]	65	50	48	15
SwSt 1	[WC9]	35	35	32	13
PM 1–188	[WC11]	35	32	12	9
IRAS 21282	[WC11]	28	26	11	9

sated by an appropriate change in $\dot{M}$ or R_*. The line profiles, however, become more and more flat-topped for an increasing wind density. This behavior explains the different results for T_* and R_t for He 2–459 and M 2–43.

The uncertainties of the results for T_* and R_t are estimated to be $\pm 10\,\%$, for v_∞ $\pm 5\,\%$. The inaccuracies of R_*, $\dot{M}$ and L depends mainly on the error margins of the distance. The element abundances of H, He and C can be determined with an error of $\pm 10\,\%$, those of O, N, Ne and Si within $\pm 30\,\%$.

The effective temperatures for He 2–459 and SwSt 1 are in excellent agreement with the results from the literature (cf. Sect. 2.2). Unfortunately, for the other objects no values from independent methods are available. The comparison of stellar temperatures derived from nebula analyses (e.g. using the Zanstra method) with our results is generally affected by the fact that in the former case the central star is supposed to radiate as a blackbody. This is definitely not the case because of strong absorption edges in the UV caused by ionization processes of He I, He II, C II or C III. The absorbed radiation is re-emitted again at infrared or even optical wavelengths. Hence, the ratio of optical flux to the number of ionizing photons, which is an important value within the Zanstra method, might be considerably larger than in the blackbody case, i.e. the Zanstra temperature of the model might be much smaller than T_*. In Table 4 the different Zanstra temperatures (for H I, He I, He II) of the models are given.

Regarding SwSt 1 we derived a relatively slow wind velocity from our analyses. The optical emission lines of He II, C III and C IV can be reproduced well by a model with $v_\infty = 400\,\mathrm{km\,s^{-1}}$. As mentioned already in Sect. 2.2 Cerruti-Sola & Perinotto (1985) found $v_\infty = 1950\,\mathrm{km\,s^{-1}}$ from low-resolution IUE spectra. Indeed, the P-Cygni shaped features of Si IV 1400 Å and C IV 1550 Å point to such high wind velocities. However, the optical emissions (e.g. C IV 5801, 5812 Å) are definitely not broadened by wind velocities of about $2000\,\mathrm{km\,s^{-1}}$. In this context it might be worthwhile to note that such broad absorption features appear also in the low-resolution IUE spectra of other [WCL] objects, e.g. NGC 40, BD+30°3639 and M 4–18. This discrepancy between UV and optical spectra cannot be solved yet, because of the lack of high-resolution UV spectra.

With the exception of SwSt 1 and IRAS 21282 the whole sample of analyzed [WCL]-type central stars (13 objects) forms a homogeneous group in which several correlations between stellar parameters are present.

Firstly, the effective temperature is correlated with the spectral subtype of the object. This is valid for the whole sample inclusive SwSt 1 and IRAS 21282. The subtype is defined by the ratio of line strengths of different carbon ions which depends not only on the effective temperature but also on the density in the wind, i.e. R_t. Thus, the correlation between temperature and subtype implies that there exist further correlations of temperature with other wind parameters.

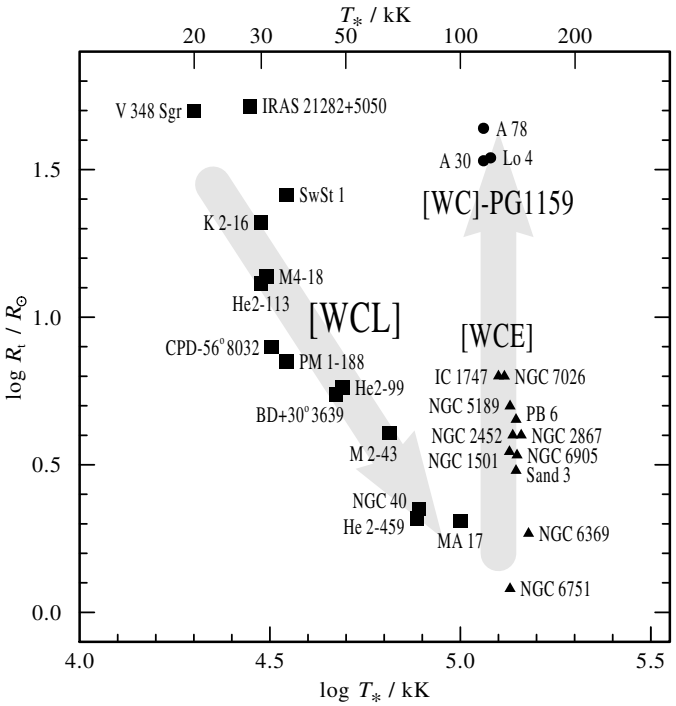

Fig. 9. Central stars of Wolf-Rayet type in the R_t-T_*-diagram. [WCL], [WCE] and [WC]-PG 1159 subtypes are represented by squares, triangles and circles, respectively. The shaded arrows suggest a possible evolutionary connection.

Indeed, the transformed radius R_t itself is interrelated to the subtype (or temperature), except SwSt 1 and IRAS 21282. In Fig. 9 this correlation appears clearly within the [WCL] group (squares in the left part of the diagram). The objects can be found along a thin strip following a $R_t \propto T_*^{-2}$ dependence (see Sect. 6 for further discussion).

Also the final velocity of the stellar wind is related to the spectral subtype. This result might indicate that the mechanism of acceleration is related to the radiation field of the central star (radiation pressure).

6. The evolutionary origin of WC-type central stars

Quantitative spectral analyses provide the empirical basis to discuss the evolutionary status of the WC-type central stars. The present paper adds five more [WCL] stars to the eight previously analyzed objects of that subclass (Paper I and II). Eleven early-type (i.e. [WCE]) stars have been analyzed by Koesterke & Hamann (1997a,b). A related spectroscopic subclass of carbon-rich central stars is termed [WC]-PG 1159 or, alternatively, Of-WR(C) or "weak emission line stars (wels)". Only three objects

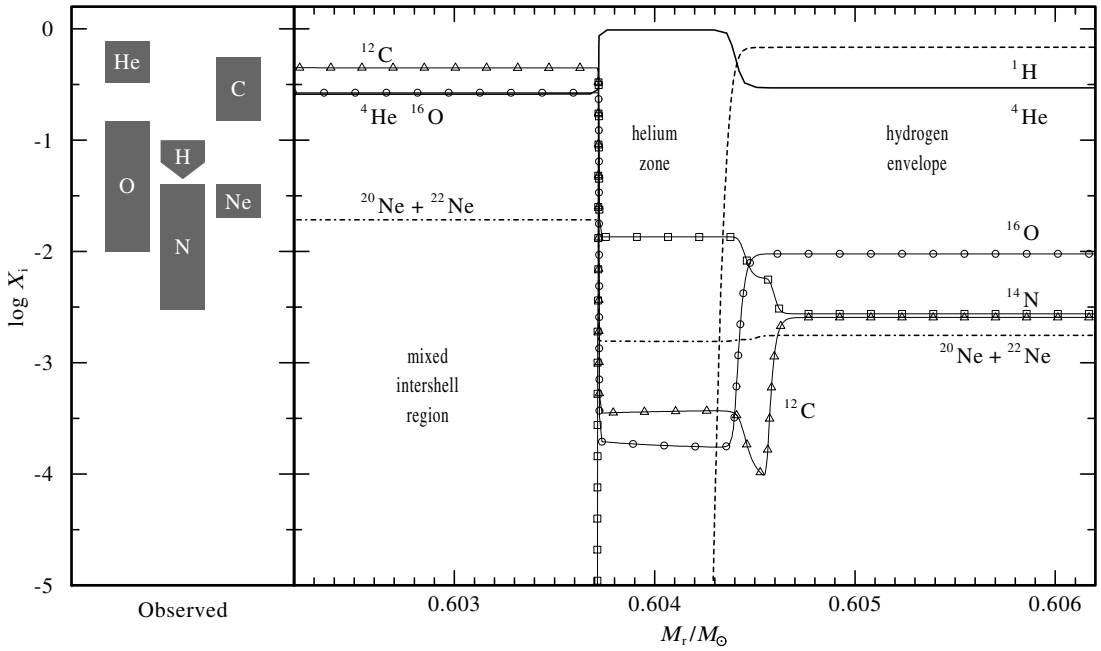

Fig. 10. The surface composition of [WC]-type central stars ([WCL] and [WCE]). The left panel indicates the ranges of surface abundances encountered within our spectral analyses. The right panel displays a chemical profile from evolutionary calculations by Herwig et al. (1997). The model star with 3 $M_\odot$ initial mass climbs the AGB and has just suffered a thermal pulse with dredge-up. The abundances (in mass fractions) are plotted versus the mass coordinate M_r (mass inside radius r). Only a small area around the hydrogen-burning shell is shown.

of that category have been analyzed so far (Werner & Koesterke 1992; Hamann & Koesterke 1993; Leuenhagen et al. 1993). While these stars still show wind signatures in their spectra, the similarly composed PG 1159 stars (for a review see Dreizler et al. 1995) do not suffer detectable mass-loss.

In Fig. 9 the parameter R_t (cf. Sect. 3) of all WC-type central stars analyzed so far are plotted versus their effective temperature T_*. The [WCL] stars form a sequence from low to high temperatures, nicely correlated with a decreasing transformed radius (i.e. increasing wind density). This good correlation ($R_t \propto T_*^{-2}$, roughly) must be inherent to the mass-loss mechanism, as the "absolute" stellar parameters L and $\dot{M}$ (possibly affected by the distance uncertainties) show a much larger scatter when correlated with T_*. Assuming an evolution at constant luminosity to higher temperatures (as in the case of H-rich CSPN) this behavior leads to the conclusion that the different subtypes of the [WCL] group form a evolutionary linked sequence [WC12] → [WC11] → [WC9] → [WC8] with a nearly constant ratio $v_\infty/\dot{M}$.

At about 130 kK the [WCE] stars are lined up at roughly constant temperature, but different transformed radii. This sequence is continued, after a gap, towards even lower wind intensities (higher R_t) by the [WC]-PG 1159 subclass. Assuming that all these stars form a continuous evolutionary sequence in that parameter plane, the path indicated by the shaded arrows is suggested. This also corresponds to a continuous path in the IRAS two-color diagram (Acker et al. 1996b).

Highly discriminating criteria for the evolutionary origin of the [WC] type central stars are provided by the observed surface composition. Central stars in general are believed to evolve from the Asymptotic Giant Branch (AGB) towards the entry of the white dwarf cooling sequence. For the CPN with hydrogen-rich surface the theoretical tracks (e.g. Schönberner 1983) are in good agreement with the empirical facts. While climbing the AGB, the stars burn hydrogen and helium in shells, and the unstable interplay between these two shell sources lead to thermal pulses which are supposed to drive the ejection of the planetary nebula. However, these thermal pulses necessarily cease *before* the hydrogen-rich envelope is totally peeled off. The star then quickly leaves the AGB, and the radiation-driven wind during the CPN stage is not sufficient to remove the remaining hydrogen layers. Thus, mass-loss alone can not cause processed material to become visible at the surface.

A solution to this dilemma is brought by the so-called born-again scenario (Iben 1984): a star which has already left the AGB may suffer a "final helium flash" which effectively mixes the remaining hydrogen envelope with deeper layers, where it is partially burned. As the occurrence of that event depends on the phase within the thermal pulse cycle when the star leaves the AGB, this scenario gives an elegant explanation for the evolutionary bifurcation into central stars of entirely different surface composition.

The task in explaining [WC] type central stars is not only to remove the hydrogen envelope, but also to prepare the observed composition *anywhere* in deeper layers which might appear at the surface in a later stage. Until recently, standard post-AGB evolutionary calculations failed to produce the observed abundance pattern at any depth. Typical He:C:O mass ratios

obtained in the intershell zone with the standard treatment are about 70:26:1, clearly discrepant from the [WC] atmospheric composition (cf. Table 2). Progress was achieved recently when Herwig et al. (1997) incorporated diffuse mixing in overshoot layers into their evolutionary code. We employ their results in the right panel of Fig. 10, displaying the chemical profile of one specific stellar model at the AGB. The mass fractions of several isotopes are plotted versus the mass inside the radius considered. The model star of Herwig et al. (1997) started life with an initial mass of 3 $M_\odot$ at the Zero Age Main Sequence. At the moment displayed here, it climbs the AGB and has just suffered a thermal pulse with dredge-up. The present mass still amounts to 2.76 $M_\odot$, while Fig. 10 shows only a small part of the chemical profile around those layers which presumably become visible at the surface during the late evolutionary stages. The envelope of the star, whose bottom is seen in the right part of the shown profile, is still hydrogen-rich. Going further inwards (i.e. towards the left in Fig. 10), steep chemical gradients mark the location of the hydrogen-burning shell. Below this shell the composition is dominated by helium. Going inwards further, another abrupt change of the chemical composition is visible. Now carbon, helium and oxygen become dominant, while nitrogen is destroyed. This material was produced by the helium-burning shell and became mixed during the past thermal pulses. Note that the helium-burning shell itself is not visible in this diagram, as it lies deeper in the star (i.e. further to the left) than the range shown here.

The left panel in Fig. 10 indicates the surface abundances which we obtained by our spectral analyses of [WCL], [WCE] and [WC]-PG 1159 stars. The filled rectangles for each element cover the whole range of mass fractions encountered in any of these stars which we have analyzed yet. For He, C, O and Ne the empirical surface abundances are in rough agreement, if we compare with the model at the mixed intershell region. More quantitatively, however, the observed helium-to-carbon ratio is generally higher than the model predicts.

Special considerations are required to reconcile the observed hydrogen and nitrogen abundances with evolutionary calculations. In their present state the models of Herwig et al. (1997) do not yet follow the post-AGB evolution. However, post-AGB stars with just the composition observed in our [WC]-type central stars are to be expected, if most of the hydrogen envelope has been removed by mass-loss and the star then suffers a "late helium flash". If the relatively thin hydrogen envelope mass is mixed with, say, a hundred times more massive interior layers, the latter will dominate the final composition, but the mixing of the former should leave characteristic signatures. One expects a small fraction of hydrogen (a few percent per mass) to survive in the outermost layers. Further inwards, the hydrogen will encounter temperatures which enforce its nuclear reaction with carbon yielding some nitrogen. These two qualitative predictions concerning hydrogen and nitrogen, including their mutual correlation (cf. Sect. 4.3), correspond nicely with our empirical results. The significant silicon overabundance, which is not predicted by the evolutionary calculations yet (Herwig et al. 1997), is another hint to additional mixing and burning processes.

Thus we expect that the new AGB models by Herwig et al. (1997), combined with envelope mixing by a "late helium flash", can explain the empirically encountered surface compositions of [WC]-type central stars.

Further constraints for the evolutionary origin of the [WC]-type central stars can be derived from the nebular ages, structure and composition (e.g. Acker et al. 1996b) or from stellar statistics. This comprehensive discussion is beyond the scope of our present paper. Moreover, binary scenarios might be considered as an alternative channel for the formation of these objects.

7. Summary

The optical spectra of five recently observed [WCL]-type central stars (He 2–459, M 2–43, SwSt 1, PM 1–188 and IRAS 21282+5050) have been utilized for spectral analyses in order to determine stellar parameters like effective temperature, wind density, final velocity of the wind and chemical composition. Together with eight further objects, which had been examined by us in the last years, 13 out of 17 known [WCL] stars (subtypes [WC8]–[WC12]) are analyzed so far using model calculations which simulate the non-LTE radiation transfer in expanding atmospheres.

The analyzed sample of 13 objects forms a homogeneous group of stars in which several correlations can be found. The subtype is strictly correlated with the effective temperature (the latest ones are the coolest). Also the final wind velocity and – with the exception of SwSt 1 and IRAS 21282 – the wind density are connected nicely to the stellar temperature (the higher the temperature the higher the final velocity and the wind density). The two objects mentioned show unusual small wind densities compared to other stars of the same subtypes.

The analyses of the element abundances (H, He, C and O are considered) yield carbon-to-helium mass ratios of about unity and oxygen contents between 1 % and 10 % (per mass). Surprisingly, hydrogen can be identified in five out of seven [WC11] or [WC12] objects. The individual hydrogen abundances scatter between 1 % and 10 % (mass fraction). Only in one star a very sharp upper limit of 0.5 % results for the hydrogen content. Principally, a safe detection of stellar hydrogen is only possible in stars of the latest subtypes ([WC11], [WC12]), because otherwise the high wind velocities cause a merging with the neighboring He II emissions. Moreover, the blending He II lines becomes greater for earlier subtypes. The large number of positive hydrogen detections within the latest subtypes (five out of seven) implies that possibly *all* [WC]-type central stars contain a small amount of hydrogen which is more or less detectable in the following stages of stellar evolution.

Objects of the latest subtypes show also features of N II, N III, Ne I, Si III and Si IV in their optical spectra. Leaving the stellar parameters from the above mentioned analyses unchanged we worked out a trace element analysis resulting in estimates or upper limits for the abundance of nitrogen (1 % at maximum) neon (2–4 %) and silicon (3 % at maximum).

Assuming a "normal" post-AGB evolution (constant luminosity, increasing temperature) our results indicate a evolution-

ary linked sequence [WC12] → [WC11] → [WC9] → [WC8]. A continuation to the [WCE] central stars (maximum of mass-loss rate), the [WC]-PG 1159 objects and finally the PG 1159 stars (no or very weak mass-loss) seems to be plausible because of similar abundance ratios at the surfaces.

Up to now a surface composition of C/He ≈ 1 together with a few percent oxygen *and* hydrogen could not be explained by evolutionary calculations. Recently examined AGB models, which include diffusive mixing during thermal pulses in the AGB phase, show a mixed intershell region located between the hydrogen and the helium burning shell. In this region the He:C:O abundance ratios are very similar to our empirical results. Supposing a late thermal pulse, which mixes the outer hydrogen-rich layer into this intershell region, the small hydrogen and nitrogen content might also be explainable.

Acknowledgements. U.L. acknowledged support from the Deutsche Forschungsgemeinschaft under grant We 1312/10-1. We thank F. Herwig, T. Blöcker and D. Schönberner for enlighting discussions and for providing us with the chemical profile of their model in electronical form.

References

Aaquist O.B., Kwok S., 1990, A&AS 84, 229
Acker A., Ochsenbein F., Stenholm B., et al., 1992, "Strasbourg-ESO Catalogue of Galactic Planetary Nebulae", European Southern Observatory, Garching
Acker A., Górny S.K., Cuisinier F., 1996a, A&A 305, 944
Acker A., Górny S.K., Stenholm B., 1996b, Ap&SS 238, 63
Bashkin S., Stoner Jr. J.O., 1975, "Atomic Energy Levels and Grotrian Diagrams. Volume I. Hydrogen I - Phosphorus XV", North-Holland Publishing Company, Amsterdam
Beintema D.A., van den Ancker M.E., Molster F.J., et al., 1996, A&A 315, L369
Cahn J.H., Kaler J.B., Stanghellini L., 1992, A&AS 94, 399
Cerruti-Sola M., Perinotto M., 1985, ApJ 291, 237
Cohen M., Jones B.F., 1987, ApJ 321, L151
Dreizler S., Werner K., Heber U., 1995, in: White Dwarfs, Proc. of 9th European Workshop on White Dwarfs, D. Koester & K. Werner (eds.), Lecture Notes in Physics, Springer Verlag, p. 160
Flower D.R., Goharji A., Cohen M., 1984, MNRAS 206, 293
de Freitas Pacheco J.A., Veliz J.G.,1987, MNRAS 227, 773
Grewing, M., Neri, R., 1990, A&A 236, 223
Hamann W.-R., 1996, Ap&SS 238, 31
Hamann W.-R., Koesterke L., 1993, in: Planetary Nebulae, Proc. of IAU Symp. 155, R. Weinberger & A. Acker (eds.), p. 87
Hamann W.-R., Dünnebeil G., Koesterke L., Schmutz W., Wessolowski U., 1991, A&A 249, 443
Hamann W.-R., Leuenhagen U., Koesterke L., Wessolowski U., 1992, A&A 255, 200
Herwig F., Blöcker T., Schönberner D., El Eid M., 1997, A&A (in press)
Hu J.Y., Bibo E.A., 1990, A&A 234, 435
Iben I. Jr., 1984, ApJ 277, 333
Jeffery C.S., 1995, A&A 297, 779
Jeffery C.S., Heber U., Hill P.W., et al., 1996, in: Hydrogen deficient stars, Proc. of 2nd International Colloquium on Hydrogen-deficient stars, C.S. Jeffery & U. Heber (eds.), ASP Conference Series Vol. 96, p. 471
Koesterke L., Hamann W.-R., 1997a, in: Planetary Nebulae, Proc. of IAU Symp. 180, H.J. Habing & H.J.G.L.M. Lamers (eds.) (in press)
Koesterke L., Hamann W.-R., 1997b, A&A 320, 91
Kwok S., Hrivnak B.J., Langill P.P., 1993, ApJ 408, 586
Leuenhagen U., Hamann W.-R., 1994, A&A 283, 567 (Paper I)
Leuenhagen U., Koesterke L., Hamann W.-R., 1993, Acta Astron. 43, 329
Leuenhagen U., Heber U., Jeffery C.S., 1994, A&AS 103, 445
Leuenhagen U., Hamann W.-R., Jeffery C.S., 1996, A&A 312, 167 (Paper II)
Likkel L., Meixner M., 1994, BAAS 185, 4701
Likkel L., Morris M., Forveille T., Omont A., 1988, A&A 198, L1
de Marco O., Barlow M.J., Storey P.J., 1996, Ap&SS 238, 91
de Marco O., Storey P.J., Barlow M.J., Crowther P.A., 1997, in: Planetary Nebulae, Proc. of IAU Symp. 180, H.J. Habing & H.J.G.L.M. Lamers (eds.) (in press)
Méndez R.H., Niëmela V.S., 1982, in: Wolf-Rayet Stars, Proc. IAU Symp. 99, C.W.H. de Loore & A.J. Willis (eds.), Reidel, Dordrecht, p. 457
Méndez R.H., Herrero A., Manchado A., Kudritzki R.P., 1991, A&A 252, 265
Mihalas D., Kunasz P.B., Hummer D.G., 1975, ApJ 202, 465
Molster F.J., van den Ancker M.E., Tielens A.G.G.M., et al., 1996, A&A 315, L373
Moore C.E., 1959, in: A Multiplet Table of Astrophysical Interest, NBS Technical Note 36
Moore C.E., 1970, NSRDS-NBS 3, Sect. 3
Nicolet B., 1978, A&AS 34, 1
Pollacco D.L., Hill P.W., 1994, MNRAS 267, 692
Preite-Martinez A., 1988, A&AS 76, 317
Preite-Martinez A., Acker A., Köppen J., Stenholm B., 1989, A&AS 81, 309
Schmutz W., Hamann W.-R., Wessolowski U., 1989, A&A 210, 236
Schönberner D., 1983, ApJ 272, 708
Shupe D.L., Armus L., Knop R.A., et al., 1994, BAAS 185, 4704
Smith L.F., 1968, MNRAS 138, 109
Swings P., Struve O., 1943, ApJ 97, 194
Tylenda R., Acker A., Stenholm B., Köppen J., 1992, A&AS 95, 337
Tylenda R., Acker A., Stenholm B., 1993, A&AS 102, 595
Werner K., Koesterke L., 1992, in: The Atmospheres of Early-Type Stars, Lecture Notes in Physics 401, Springer Verlag, p. 288
Zhang C.Y., Kwok S., 1991, A&A 250, 179
Zijlstra A.A., Gaylard M.J., te Lintel Hekkert P., et al., 1991, A&A 243, L9

This article was processed by the author using Springer-Verlag LaTeX A&A style file *L-AA* version 3.